Material-Tailored Thermo-Mechanical Design

in the RTO / AVT Lecture Series "Engine Intake Aerothermal Design"

Hannah Böhrk
Institute of Structures and Design
DLR, German Aerospace Center
November 2011

Preface

Leading edges, as they appear for example in hypersonic airbreating engine intakes or vehicle "noses", are subjected to severe aerodynamic heating. Their thermo-mechanical design is, among others, a key discipline to optimum hypersonic vehicle design.

The Institute of Structures and Design (Institut für Bauweisen und Konstruktionsforschung, BK) of German Aerospace Center (Deutsches Zentrum für Luft- und Raumfahrt, DLR) develops CMC material and advances thermal protection systems for atmospheric re-entry vehicles. The fiber ceramic C/C-SiC used for the SHEFEX II TPS is manufactured in house at DLR-BK. It is a composite consisting of carbon fibers with a matrix of carbon and silicon carbide. It has been qualified in plasma wind tunnel testing and during real re-entry flight, such as in the FOTON 9, EXPRESS, FOTON-M2, and SHEFEX missions.

The present work is based on and profits from this broad experience. Fruitful help was provided by my colleagues Hendrik Weihs, Thomas Reimer, Markus Selzer, Christian Dittert, Henning Elsäßer, Dr.-Ing. Hermann Hald, Dennis Zink and Dr.-Ing. Stefan Löhle.

Chapter 1 gives an overview over the loads on hypersonic vehicles, putting into relation the two typical hypersonic flight situations atmospheric re-entry flight and hypersonic cruise flight. In chapter 2, thermal protection strategies are discussed and an approach of determining thermal protection system temperature for their proper layout is given. From the occuring loads and requirements for thermal protection systems, requirements on the material choice can also be derived. Chapter 3 gives a brief overview over metallic and ceramic materials and explains advantages for fiber-reinforced ceramics, the ceramic matrix composites. Based on this material, chapter 4 gives design examples in which both thermo-mechanical and material-tailored design rules are implemented. The examples are given based on former and ongoing projects at DLR-BK. Finally, in the last chapter, sharp leading edges are discussed with respect to passively or actively cooled leading edges and an overview of activities within DLR, but also external, is given.

However, the development of leading edges is ongoing and the examples shown here make no claim to be complete. New and improving solutions are, therefore, rather possible. Have you got an idea?

Hannah Böhrk

Inhaltsverzeichnis

1 Hypersonic Flight

Hyperconic velocities are encountered in the two typical flight situations

- atmospheric re-entry flight
- hypersonic cruise flight.

Both are connected with flight in the atmosphere, where the large velocities of the vehicle causes a shock or a bow wave ahead of the vehicle. Through this shock, the atmospheric gas is compressed and the kinetic energy is dissipated into internal energy of the atmospheric gas. In case of an Earth re-entry, an air plasma state is formed in the surrounding gas which is characterized by high temperatures and dissociated and partly ionized particles. Air temperatures can reach up to 20'000 K with a compression ratio p_{tot}/p_∞ of several hundred.

Hypersonic velocity is generally defined as velocities of Mach >5 and implies effects like narrow shocks with shock distances so small that the shock layer may interact with the boundary layer or high temperature effects in which the atmospheric gas is decomposed by dissociation of the molecules and ioniziation of flow particles. It was found in the 50s by H.J.Allen that the shock distance δ to the vehicle surface increases with the nose radius which drastically decreases heat load. Oertel [2] gives the correlation

$$\delta = 2R\left(\frac{0.099(\kappa+1)}{M^2}\right)^{2/3} \tag{1.1}$$

for transsonic and

$$\delta = 0.143 Re^{3.24/M^2} \tag{1.2}$$

for hypersonic flight with the isentropic coefficient κ and Mach number M.

A few vehicles foreseen for re-entry missions are shown in figure 1.1. Typical entry velocities range from 7.9 km/s for an Earth orbital re-entry, over 11.3 km/s for a return mission from Moon or 15 km/s for a return from Mars. The kinetic enthalpy is given by

$$h = \frac{1}{2}v^2 \tag{1.3}$$

which amounts to approximately 31 MJ/kg, 63 MJ/kg and 110 MJ/kg, respectively.

Re-entry vehicles are in principle deceleration systems, the most prominent one being the Space Shuttle [3]. Therefore, all of these vehicles are rather blunt in order to achieve large drag and a large shock distance ahead of the vehicle. Throughout the distance from shock layer to vehicle surface, the energy is dissipated into internal degrees of freedom of the atmospheric gas, like dissociation, vibration or rotation. This causes a reduction of the sensible temperature of the gas for the vehicle surface and the nose radius is thus chosen large. Among the re-entry vehicles, non-winged and winged vehicles are differenciated, comprising ballistic and lifted trajectory

Figure 1.1: Re-entry vehicles: a) Apollo, b) Stardust which has performed hyperbolic re-entry in 2006 after having collected dust from the coma of comet Wild 2, c) European re-entry vehicle ARD (Atmospheric Re-entry Demonstrator) which has completed re-entry flight from a sub-orbital mission after launch with Ariane 5, d) Space Shuttle operated on 135 missions from 1981 to 2011.

strategies, respectively. The challenge of the atmospheric re-entry is that the vehicle needs to slow down from 7.9 km/s, i.e. 28'000 km/hr, to 0 km/s on the ground by only atmospheric deceleration in terms of drag and friction. This can be achieved by the ballistic trajectory in which the vehicle falls at high velocity back into the atmosphere and thus encounters strong deceleration loads and a high heat flux onto the material during the short time of the re-entry. It may, however, also be achieved by a lifted re-entry, in which the strategy is to decrease velocity at higher altitude, where the atmosperic density is still relatively low, and thus encounter only a reduced amount of heat flux. In figure 1.2, both re-entry strategies are sketched. However, when staying at elevated altitude, the mission time is increased and the vehicle has to withstand the reduced heat flux during a longer period of time. Figure 1.3 shows the heat flux over time for the capsule mission EXPRESS (blue with symbols) in comparison with the heat flux for winged re-entry body X-38 (orange with symbols). The winged body is set out to lower heat load but during a longer period of time. The integral under the two curves, since their entry enthalpy is comparable, is comparable, too.

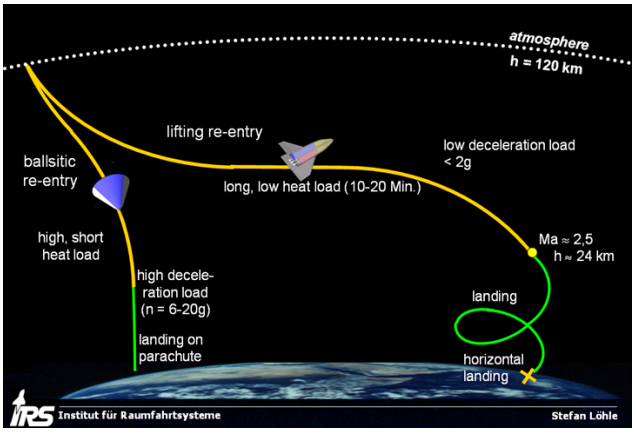

Figure 1.2: Ballistic and lifted re-entry strategies [Löhle, IRS].

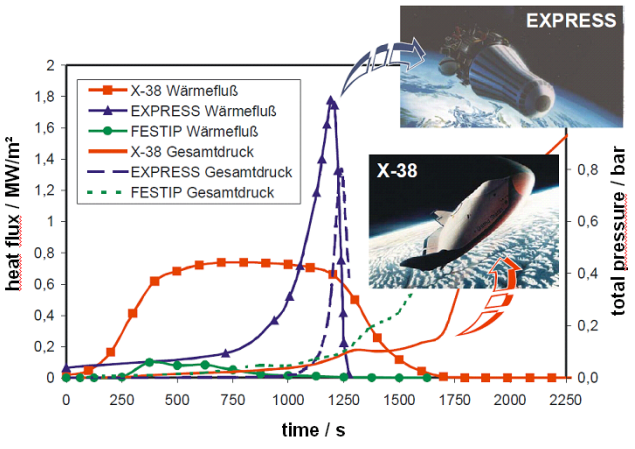

Figure 1.3: Heat flux and total pressure for a ballistic (EXPRESS) and a lifted (X-38) re-entry flight.

Capsule type re-entry bodies typically have axissymmetric shape and fly at negative angle of attack, resulting in weak aerodynamic performance, the measure of which is the lift-to drag ratio L/D. This parameter governs mission capabilities like down- and cross range. Figure 1.4 shows cross range capabilities of hypersonic vehicles.

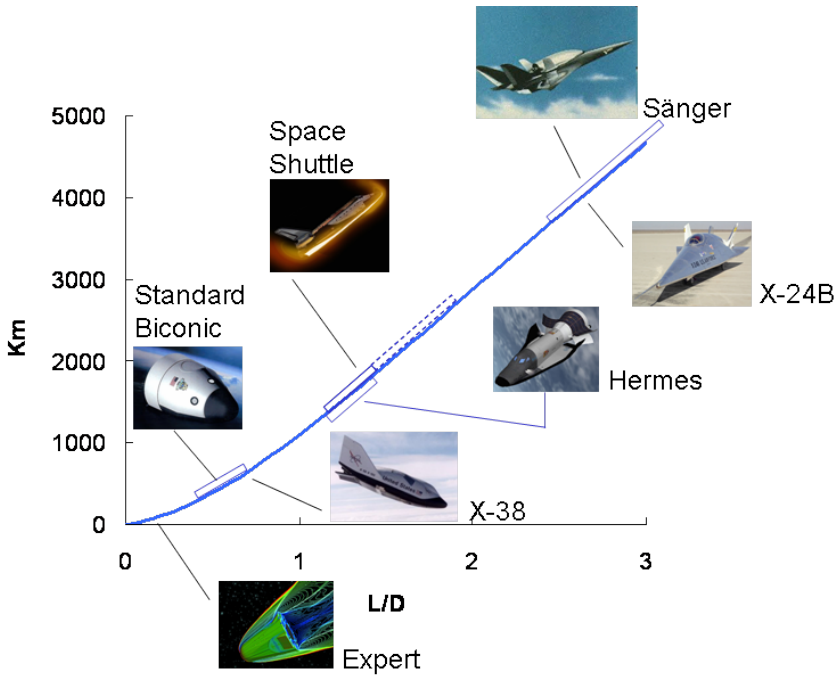

Figure 1.4: Cross range capabilities for hypersonic lift- over-drag ratio for various hypersonic flight vehicles.

Winged re-entry bodies have rather flat lower sides and fly at large postitive angles of attack, resulting in an aerodynamic performance L/D between 0.5 and 2.

Opposed to re-entry vehicles, hypersonic cruise vehicles must, aircraft-like, fly with efficient propellant consumption. These vehicles are not operational, so far. The technology however, evolves. Major recent milestones were the X-43 flights in 2004 with M=6.83 and 9.68 [3]. Hypersonic cruise vehicles have to have minimum aerodynamic drag in order to be propellant efficient, which for hypersonic flight necessitates a slender configuration. Equation 1.2 shows that a shock stands ahead of blunt shapes but may be attached to pointed shapes, showing that leading edges of hypersonic cruise vehicles see very high heat load.

A formulation by Zoby is widely used for determining heat flux

$$\dot{q} = K \times 10^{-4} \sqrt{\frac{p_{tot}}{R_{\text{eff}}}} h \tag{1.4}$$

for the stagantion region of a hypersonic vehicle with flight enthalpy h, efficient nose radius R_{eff}, total pressure p_{tot} and the gas specific constant K, which is $0.368\,\text{kW kg}\,(\text{MJ m})^{-1}(\text{m Pa})^{-1/2}$. The heat flux to the leading edge is depending on the leading edge radius proportional to a root function, as depicted in figure 1.5.

From an aerothermodynamic point of view, sharp leading edges hold problems. They promote local stagnation areas with very high temperatures, that have not been withstood by materials, before. However, sharp leading edges are also known to have minimum drag, require relatively low thrust during ascent or cruise flight and achieve higher cross-range leading to mission flexibility, as opposed to blunt bodies. During the 1990s, the development of ceramic composite and ultra high temperature materials for TPS applications led to a renewed interest in sharp edged configurations [4] such as the waverider concept DLR F8[5], the DLR-ONERA project JAPHAR [6] or the lifting body concept HL-20 and the SHARP project, both from NASA [7, 8].

Both, atmospheric re-entry vehicles and hypersonic cruise vehicles, therefore, need a thermal protection system. Figure 1.6 shows what happens at atmospheric re-entry without a heat shield. ATV (Automated Transfer Vehicle), the European expendable supply spacecraft has been brought to a destructive re-entry in the atmosphere on purpose. As the density increased upon re-entry, the heat load reached the maximum temperatures the materials can withstand and it separated into three major fragments. It is supposed that the equipment bay has first collapsed, followed by the propellant bay and lastly the cargo bay. The part that survived the longest time was the russian docking adapter, a massive titanium component.

The TPS designer must account for the thermo-mechanical loads onto the vehicle. However, since access to space is costly, overdesign must be avoided. Therefore, the TPS designer needs to lay out the heat shield against transient loads, considering also the heat capacity of the heat shield material. The extreme temperatures experienced in the nose and leading-edge regions of ultra-fast concepts require advanced cooling.

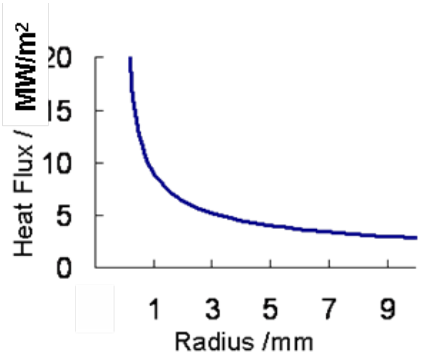

Figure 1.5: Radiative equilibrium heat flux.

Figure 1.6: ATV burn-up during re-entry [NASA]

2 Thermal Protection Systems

Thermal protection systems (TPS) are required for a range of hypersonic vehicles ranging from ballistic reentry to hypersonic cruise vehicles. The TPS designer must account for the thermo-mechanical loads onto the vehicle. However, since access to space is costly, overdesign must be avoided. Therefore, the TPS designer needs to lay out the heat shield against transient loads, considering also the heat capacity of the heat shield material.

There are multiple options for dealing with the severe thermal environments encountered during hypersonic flight. Included in these critical components are leading edges, control surfaces, acreage TPS, and seals, as illustrated in figure 2.1.

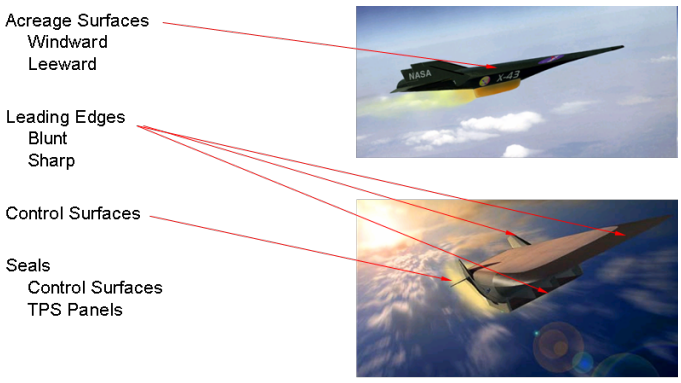

Figure 2.1: TPS components.

Depending on the boundary conditions of the mission, passively and actively cooled approaches can be utilized. Figure 2.2 shows, with relation to the diagram of figure 2.3, which strategy must be used.

In oder to lay out and design the TPS, the thermal response of the material to the load has to be determined. Depending on the mission, transient wall temperature determination is essential in order to optimize TPS mass. However, for horizontal hypersonic cruise flight at likely invariant flight condition and atmospheric condition, a steady state of the TPS is approached.

The heat equation

$$\rho_{mat} c_{p,mat} \frac{\partial T}{\partial t} = \lambda_y \frac{\partial^2 T}{\partial y^2} + \lambda_x \frac{\partial^2 T}{\partial x^2}\,, \tag{2.1}$$

can serve as an approach to describe the temperature development at any point within the TPS material. In case of a steady-state problem $\frac{\partial T}{\partial t}$=0. Boundary condition is the heat balance at the surface and a boundary condition of second order can for example be used at the rear side and the edges of the TPS-panels

$$\lambda_y \left(\frac{\partial T}{\partial y} \right)_W = 0\,, \tag{2.2}$$

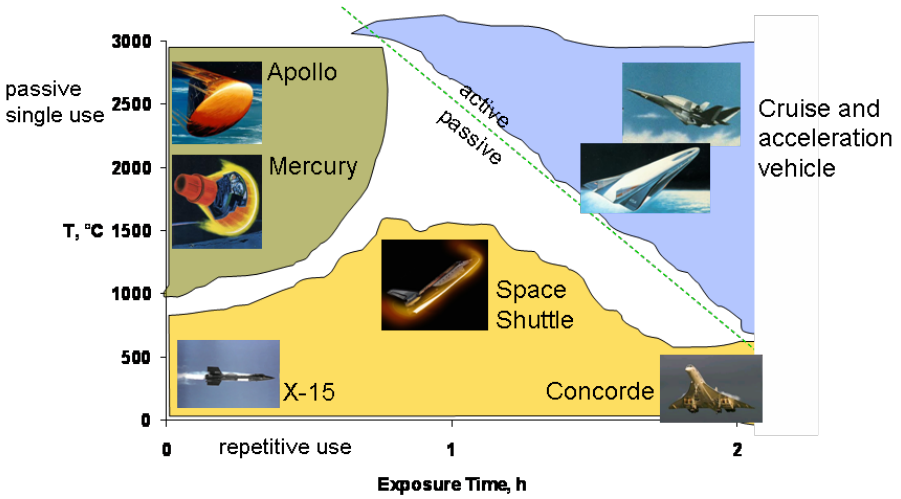

Figure 2.2: Boundary conditions in which active and passive thermal protection systems are needed.

i.e. assuming that these sides are adiabatic.

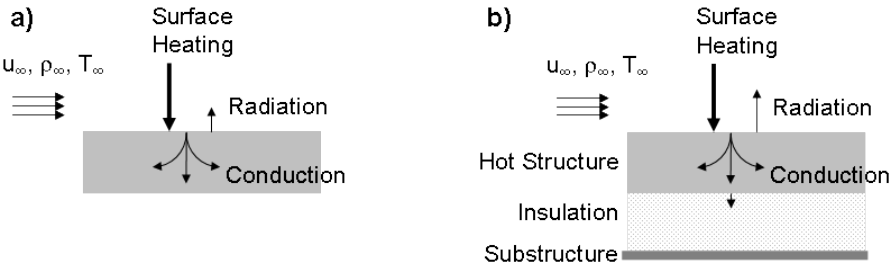

Figure 2.3: a) Capacitive cooling and b) radiation cooling.

Figure 2.3 a) illustrates a capacitively cooled thermal protection system that manages the heat by a thick wall and high heat conductivity and -capacity. This is used for low heat fluxes and relatively short mission times and is located in the lower left of figure 2.2. Because of relatively low wall temperature, radiative cooling with

$$\dot{q}_{rad} = \sigma \epsilon T^4 \tag{2.3}$$

with Stefan-Boltzmann-constant σ and the wall material's emissivity ϵ, is marginal. If a heat sink structure is heated for a long period of time, enough heat could be absorbed to overheat the structure. The example shown in fig. 2.2 is with the X-15, where the leading edges utilized a heat sink structure [1].

Figure 2.3 shows in b) a radiatively cooled system which is used for example in the EXPERT nose cap or SHEFEX. More details on these missions follow in chapter 5 and a view of the SHEFEX TPS is given in figure 4.11.

Thermal radiation as the mechanism to remove the heat becomes more efficient with higher temperature. The emission coefficient has strong influence on the surface radiation cooling. Figure 2.4 shows the radiation heat flux emitted away from the vehicle surface according to wall temperature, emission coefficient according to equation 2.3. In contrast to a heat sink structure, hot structures can be used for a higher heat load for long times, allowing the structure

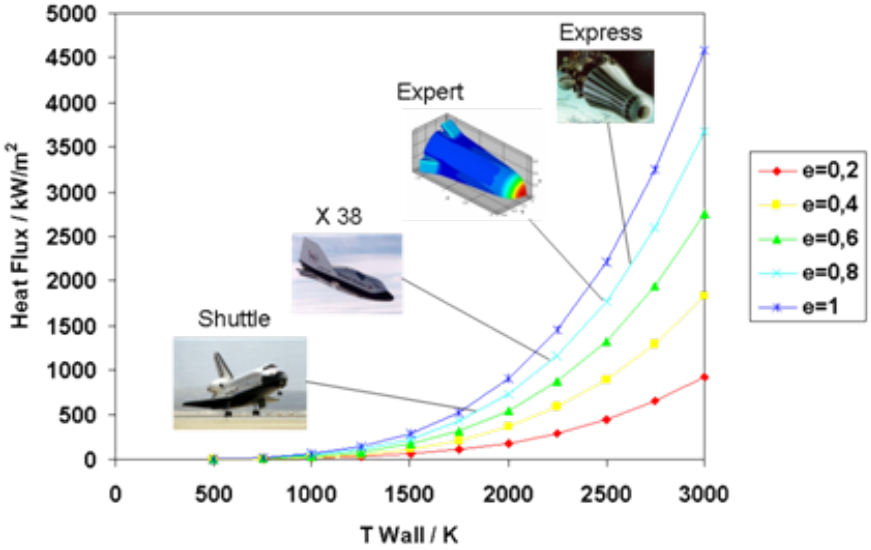

Figure 2.4: Radiation heat flux.

to reach steady state conditions. Again, the heat is both radiated away and conducted inward. The objective of the insulation is to minimize heat reaching the structure, which remains cool. Figure 2.3 indicates that a small amount of heat is conducted through the insulation to the structure. In this case, boundary condition (2.2) can change into heat conduction through a stacked pile of material until on the inside of this stack there is again the adiabatic condition.

The heat balance for the surface in case of the capacitively and radiatively cooled assumes that all incoming heat flux $\dot{q}_{HG-W}$ from the hot gas to the wall is either conducted into the structure by $\dot{q}_{cond}$ or radiated away with $\dot{q}_{rad}$ so that is [9]

$$\dot{q}_{HG-W} = \dot{q}_{rad} + \dot{q}_{cond}\,. \tag{2.4}$$

Heat flux from the flow to the wall can be convective heat flux, radiation or chemical effects like catalysis. In the present approach these effects are neglected and only convective heat flux is looked at. The thermal energy

$$\dot{q}_{HG-W} = \alpha_A\,(T_r - T_W) \tag{2.5}$$

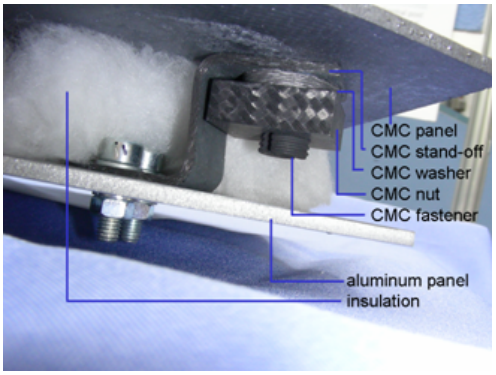

Figure 2.5: SHEFEX II thermal protection system set-up.

is transferred from the hot gas to the wall through convection with the areal heat transfer coefficient α_A and the recovery temperature T_r. These parameters are functions of the flow properties and can be expressed as

$$\alpha_A = St\rho_\infty c_{p,\infty} u_\infty \tag{2.6}$$

and

$$T_r = T_\infty \left(1 + r\frac{\kappa - 1}{2} M_\infty^2\right). \tag{2.7}$$

The two commonly unknown variables of eqs. (2.6) and (2.7) are the Stanton number St and the recovery factor r. They must be determined for each flow condition, be it laminar or turbulent. This can done based on known models of Crocco and van Driest [9, 10, 11] The last boundary condition is

$$\dot{q}_{cond} = \lambda_y \left(\frac{\partial T}{\partial y} \right)_W . \tag{2.8}$$

In a radiation adiabatic and therefore steady state, this heat flux equals zero.

If high heat flux has to be sustained for long times, a semi-passive thermal protection approach may need to be utilized. A heat pipe could be used for high heat fluxes for long periods of time. Heat is transferred by a working fluid to another region of the heat pipe where the heat is radiated away. The heat pipe system was describen by Glass in [1]. A copy of his paragraph is given for further description in the leading edge section 6.2.1. Figure 2.6 shows the heat transfer mechanisms for the heat pipe. All processes remain the same as with radiative or capacitive cooling remain, but the boundary condition (2.2) on the inside of the heat pipe turns into another heat balance

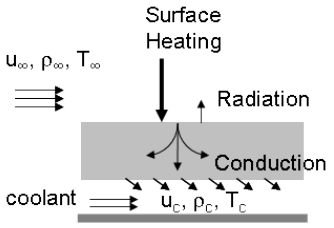

Figure 2.6: Heat pipe cooling.

$$\dot{q}_{cond} = \dot{q}_{W-C} + \dot{q}_{rad} \, , \tag{2.9}$$

with index $W - C$ indicating convective heat transfer from the wall to the coolant. Heat flux $\dot{q}_{W-C}$ can, again, be estimated as $St\rho_c c_{p,c} u_c (T_W - T_{r,c})$.

active cooling is required for even higher heat flux and for long mission times. The region is located in the upper right in figure 2.2. Convective cooling, in which the coolant heats up and carries the heat away, is often utilized for a high heat flux and long times. The structure operates hot but is maintained within its temperature use limits by the active cooling. Two kinds of convective cooling, film and transpiration cooling, are sketched in figure 2.7.

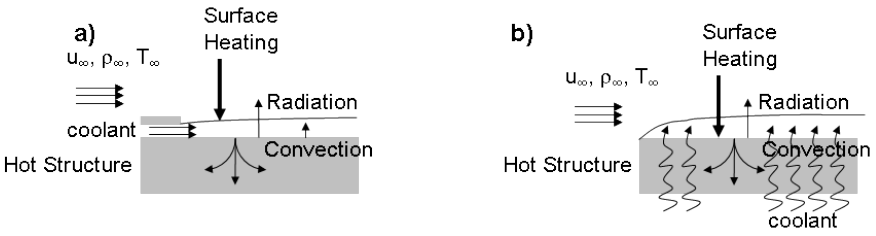

Figure 2.7: a) Film cooling and b) transpiration cooling.

For film cooling, the coolant is injected into the flow at a disrete upstream location. It blocks off the heat flux from the wall like a thin, cool, insulating blanket. The surface heat balance, equation (2.10) turns into

$$\dot{q}_{F-W} = \dot{q}_{rad} + \dot{q}_{cond} \tag{2.10}$$

with index $F - W$ indicating convective heat transfer from the coolant film to the wall. Then, in order to determine the film temperature, another boundary condition is needed. Heat flux

from the hot gas $\dot{q}_{HG-F}$ heats up the film which in turn heats the wall over a TPS length Δl. At the same time, cool flow with flow enthalpy h_{in} is flowing in from upstream and is heated up before it exits the film of film thickness δ_F on the downstream side with increased flow enthalpy h_{out}

$$(\dot{q}_{HG-F} - \dot{q}_{F-W})\,\Delta l = ((\rho u h)_{out} - (\rho u h)_{in})\,\delta_F. \tag{2.11}$$

Turbulent flow is characterized by a strong vorticity, leading to a mix between the two gas flows, hot and film, and reducing the cooling efficiency. In the heat balance of the coolant film as of eq. (2.11), the term of convection between hot gas flow and film can be replaced by a a term $\dot{m}h_\infty$ accounting for the entraining hot gas mass into the film and the subsequent heat adjustment between the fluids. Equation (2.11) becomes

$$\dot{m}h_\infty - \dot{q}_{F-W}\Delta l = -\left(h\rho u\right)_{in}\delta_{in} + \left(\left(\rho u\right)_{in}\delta_{in} + \dot{m}\right)h_{out} \tag{2.12}$$

with growing film thickness δ_F. The factor $\dot{m}$ describes the mass of air entering into the film [9].

In transpiration cooling, a coolant is transpired through a porous and permeable wall structure to the outer mold line of a TPS and there forms a film like with film cooling. Incontrast to the discrete locations used in film cooling, this is done over large areas. The structure is cooled by both convection as the coolant passes through the pores and by the coolant wall flow, i.e., film, on the hot-gas side. The heat balance is thus that of above for the laminar or the turbulent flow condition. The cooling of the inner structure of the porous material is carried out by convective heat transfer between the material and the coolant. Radiation within the porous structure is neglected. According to Glass, the balance for the wall material is [12]

$$\lambda_x\frac{\partial^2 T_{mat}}{\partial x^2} + \lambda_y\frac{\partial^2 T_{mat}}{\partial y^2} - \alpha_V\left(T_{mat} - T_F\right) = \rho_{mat}c_{p,mat}\frac{\partial T_{mat}}{\partial t} \tag{2.13}$$

and the one for the gas, accordingly,

$$-\frac{\partial\left(\frac{\dot{m}(x,y)}{A}c_{p,F}T_F\right)}{\partial x} - \frac{\partial\left(\frac{\dot{m}(x,y)}{A}c_{p,F}T_F\right)}{\partial y} - \alpha_V\left(T_{mat} - T_F\right) = \rho_F c_{pF}\frac{\partial T_F}{\partial t}\,. \tag{2.14}$$

When only the pressure gradient in flow direction is taken into account the above equation yields

$$-\frac{\dot{m}}{A}\frac{\partial\left(c_{p,F}T_F\right)}{\partial y} - \alpha_V\left(T_{mat} - T_F\right) = \rho_F c_{pF}\frac{\partial T_F}{\partial t}, \tag{2.15}$$

with the volumetric heat transfer coefficient α_V.

Ablation is another semi-passive approach to thermal management. The purpose of the ablator is to keep the structure cool. Ablators are utilized for very high heat fluxes, but for relatively short times, and are for single use. As an example, an image of the Orion capsule is shown in Figure 8, which includes an ablative heat shield. This is the same approach that was used on the Apollo capsule, where the heat is blocked by ablation and the ablator is consumed. Heat is also absorbed by the ablation process.

3 Material Choice

In the previous section, passive and active thermal protection systems have been described. They consist of structural parts, hot structural parts, attachment components and a system infrastructure (e.g. gas or liquid reservoir for active cooling). Flight vehicle substructures are commonly metal frames with good thermal conductivity, so that hot spots are avoided where hot parts are attached. The materials of the hot structures should typically by

- high-temperature capable, i.e. materials must not melt or soften at elevated temperature
- of low mass, i.e. density
- of high specific strength and stiffness
- of high emissivity
- of low heat conductivity when insulated hot structures are used
- of no or low erosion rate, e.g. due to oxidization or nitridization
- of low surface catalycity, i.e. enhancing recombination of atomic species at material surface
- of compatible thermal expansion with their substructure

Metallic materials that can be used in thermal protection systems are for example γ-titanium-aluminates, β-titanium or high performance NiCr-alloys. The latter are for example Inconel, dispersion strengthened steel PM1000 or Haynes. Figure 3.1 shows the metallic thermal protection system MERIT by Astrium. It sustains temperatures to 900°C. Earlier γ-titanium-aluminate TPS were made to withstand 600°C. However, thermal expansion limits size and causes thermally induced deformation and loss of strength at increasing temperature.

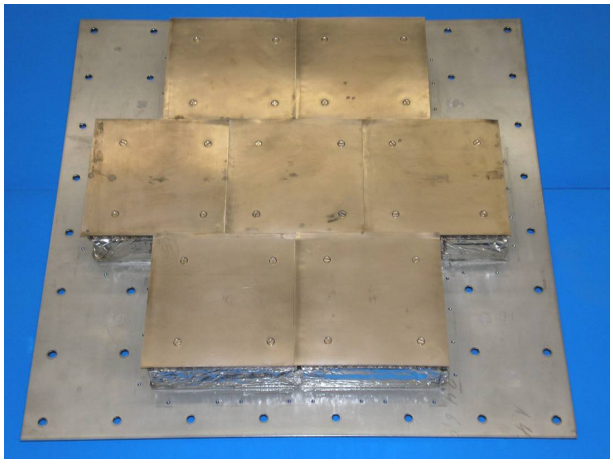

Figure 3.1: Metallic TPS from β-Titanium from EADS Astrium.

For the severe heat load at leading edges, metallic TPS still have to meet higher temperatures or they have to be actively cooled. Another high temperature material option are ceramic materials. Ceramics are difficult to define, they are mostly categorized by the exclusion principle: they are inorganic nonmetallic solids with cristalline or amorphous microstructure. They are cured under heat and are thus, naturally, heat resistant at least up to their cure temperature, but often even beyond after subsequent cooling.

Ceramic material can be used in components or as coatings on other parts. The fabrication process of components follows the sequence

- milling and mixing
- forming of a "green body" for example in a press
- sintering

as depicted in figure 3.2. The sintering, i.e. firing, is done below the melt temperatures of the

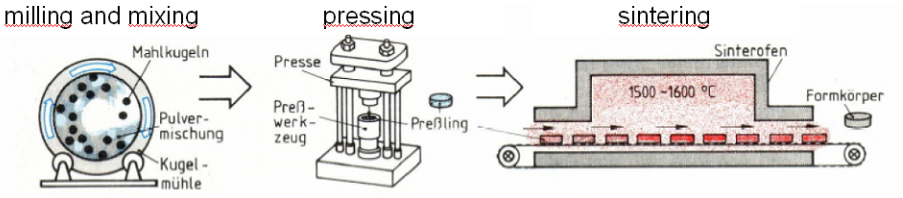

Figure 3.2: Processing steps in ceramic fabrication, source: Prof. Bozena Arnold.

ceramic. Atomic and molecular diffusion processes during this process step cause changes in the primary microstructural features. Figure 3.3 symbolizes how porosity is eliminated which is typically accompanied by a net shrinkage and overall densification of the component. The densified object also embodies higher strength and fracture toughness. However, in repetition parts, a compromise must be found between strength of the component and efficient production.

Ceramics are generally divided into the groups of oxides and nonoxides. Typical candidates used in aerospatial applications are aluminium oxide (Al_2O_3, alumina), zirconium oxide (ZrO_2, zirconia) and silicon carbide (SiC). Metal diborides and their composites, known as ultra high temperature ceramics (UHTC), have gathered substantial interest, being able to withstand temperatures above 3000°C. Examples are ZrB_2 and HfB_2.

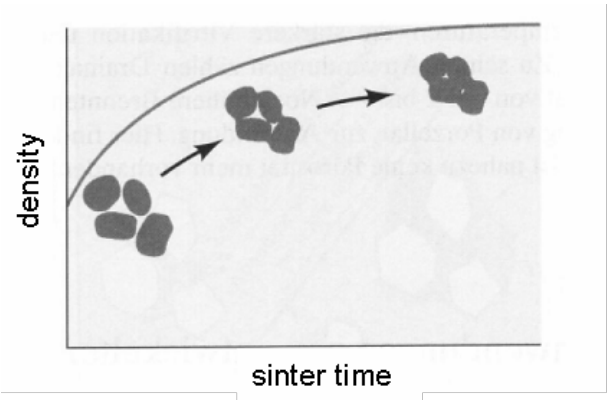

Figure 3.3: Schematic of densification during sintering.

Figure 3.4 gives an overview of a range of monolithic ceramics in comparison to a standard aluminium and titanium. It shows that they all range in several g/cm^3 with the UHTCs being heaviest. The oxidic ceramics are good electric and thermal insulators with aluminum oxide at few ten W/mK and zirconia at only a few W/mK. Silicon carbide, in contrast, is a "good" (i.e. relatively good) thermal conductor with over a hundred W/mK. This thermal conductivity is higher than that of steel, however, it is only half that of aluminum. All ceramics have low thermal expansion, the highest one in the choice here being zirconia which makes it a material that can be joined with steel, if a coating or clutch is needed. All of these ceramics are chemically

inert, wear resistant with good tribologic properties. Alumina is relatively priceworthy with good shaping and sizing capability.

	Al-6061	Ti-6-4	SiC	Al_2O_3	ZrB_2	HfB_2
density at 20°C (g/cm³):	2,7	4,43	3,1	3,96	6,1	11,2
melt temperature (°C):	582	1604	2700	2072	3245	3380
tensile strength (MPa):	310	1170	-	-	-	-
Young's Modulus (GPa):	68,9	114	410	400	489	480
thermal conductivity (W/mK):	235	6,7	110	27	60	104
thermal expansion (10^{-6}/K)	23,1	8,5	4	8	5,9	6,3

Figure 3.4: Metallic and monolithic ceramics typical material propoerties at standard conditions (p=1 atm, T=20°C).

Since monolithic ceramics typically offer no damage tolerance, they typically fail in a catastrophic way after overloading. Cracks initiated by flaws, e.g. pores and surface defects, cannot be stopped and therefore run through the complete part. Due to the fact that the number of flaws is increasing with the volume of the ceramic part, the failure probability of large structures is higher than that of small parts, leading again to a reduced allowable stress level and high wall thicknesses of structural parts. Monotlithic ceramic components are, therefore, mostly small and simple shaped with rounded edges in order to avoid stress peaks. They are very brittle and can be well compression loaded but endure only little tensile load. Since bending moments cause tensile stress in some parts of the component, large parts are difficult to maintain. When using ceramics in structural parts, care must therefore be taken at the mechanical interfaces with parts. Loads have to be introduced into the parts rather with compression than tension, for example by clamping, and without the risk of inducing stress peaks.

Ceramic material is a good candidate for thermal protection systems because of its temperature resistance. However, it is difficult to design and manufacture for structural parts and parts loaded with large temperature gradients because of its brittle nature. Material flaws and machining may introduce microcracks that will cause early fracture. More reliability can be achieved with embedded fibers in a ceramic matrix. In contrast to monolithic ceramics, where the apprearance of cracks will directly destroy the structure, the cracks within a fiber reinforced composite material enable a degradation of stress peaks giving the material a good tolerance. Figure 3.5 shows how fibers in a ceramic laminate can act as a crack stopper.

While in monolithic ceramics a pure substance is aimed for, ceramic matrix composites (CMC) are multicomponent materials. In the monolithic part one would always strive for small grain size, perfect grain boundaries and elimination of cracks, defects or pores. Meanwhile, the fiber reinforced material develops a micro crack pattern. Emerging cracks can be stopped at the fibre/matrix interface and at micro pores. Therefore, the strength of CMC materials is independent from the component size, enabling the realization of mechanically and thermally extremely loaded, large sized and thin walled lightweight structures. CMCs have weak fiber-matrix bonding and higher matrix modulus than fiber modulus. This results in an improved damage tolerance due to the fiber pull-out. Since CMC are lightweight and have stable properties with respect to Young's modulus, strength, stiffness and tensile stretch even at high temperatures, they are much applied for thermal protection outer skins. It was understood already above that the fibers enhance damage tolerance of ceramics and it can be seen from the table that they increase the ceramic material's tensile strength while still being temperature and wear resistant. They also reduce the thermal expansion of the material. This is useful in structures that are subject to large thermal gradients, so thermal stresses do not affect the

component a lot. With the structural properties of these materials, it is possible to manufacture ceramic parts that are even thin-walled, large or complexly shaped.

An example for a CMC material, C/C-SiC, is shown in figure 3.6. The material is based on carbon fibers with a carbon and silicon carbide matrix. The fiber lay-up is typically a stack of 0/90°planar laminae so that the material is directional. Within the laminae planes and parallel to the fibers are the 0°and 90°direction, while the material can also be oriented ±45°or any other angle. It has relatively low porosity of 3% at low overall density. The thermal expansion is low in laminae direction and a little higher perpendicular to the laminae. The values are given in figure 3.7. The material has high specific strength at high temperature and is thermo-shock resistant. Since it is made with carbon fibers it has mediocre oxidation resistance.

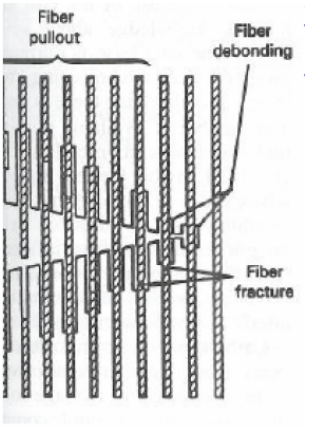

Figure 3.5: Fibers acting as crack stoppers within a ceramic matrix.

C/C-SiC has been qualified in plasma wind tunnel testing and during real re-entry flight, such as in the FOTON 9 [13], EXPRESS [13, 14], FOTON-M2 [15], and SHEFEX [16, 17] missions. The nose cap of the X 38 was developed, constructed and set up [18]. Recently, the nose TPS for EXPERT [19], a project of the European Space Agency (ESA) and the follower of SHEFEX, SHEFEX II, are developed at DLR-BK. It withstands load up to high temperatures of 1840 K. Moreover, with large damage tolerance it is highly resistant to thermo-shock and nearly oxidation resistant at low thermal expansion of $2\times10^{-6}\,K^{-1}$ parallel and $6\times10^{-6}\,K^{-1}$ perpendicular to the fiber.

The fiber ceramic C/C-SiC is manufactured in house at DLR-BK [20]. The process is described here as an example for the manufacturing of CMC complonents. In a first step, a green body is made from carbon fiber reinforced plastic. Secondly, the green body is treated by pyrolysis under a pure nitrogen atmosphere at 1170 K and, thus, the matrix is carbonized to C/C. This intermediate stage C/C has intriguing permeable properties. In the latter (second) step, a micro crack pattern is formed within the carbon matrix. The third step contains the liquid infiltration of the C/C-body with silicon under vacuum at 1870 K. Silicon carbide is formed beginning at the phase interfaces between silicon and carbon until the entire matrix is transformed to silicon carbide, meanwhile the fibres remain unaffected and a content of free silicon of ≈2% remains.

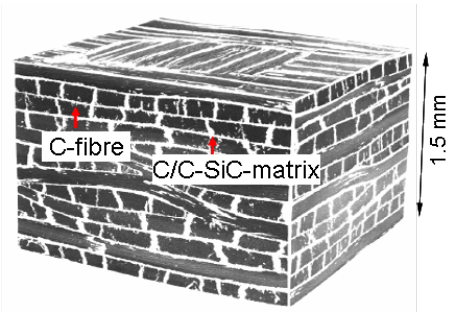

Figure 3.6: Micro structure of C/C-SiC.

	Tenax	Nextel 610	C/C-SiC	C/SiC	Whipox
Density at 20°C (g/cm³):	1,76	3,96	1,9	2,1...2,3	1,5...3
tensile strength (MPa):	3950	3144	-	-	-
flexural strength (MPa):	-	-	80	270...33	55...120
Young's Modulus (GPa):	238	375	60	90...100	40...200
Thermal conductivity (W/mK):	17	-	ll 8,5 ⊥9	ll15 ⊥7	0,5... 5,7
Thermal expansion (10^{-6}/K)	-0,1	7,9	ll -1 ⊥2,5	ll 2 ⊥5	4,3... 8,4

Figure 3.7: Material properties of fibers (Tenax carbon fiber and Nextel alumina fiber) and CMC materials: C/C-SiC, C/SiC as published by M. Leuchs from MT Aerospace (2006) and WHIPOX, CMC from alumina fibers with alumina matrix.

4 Material-Tailored Thermo-Mechanical Design

The examples above have shown that design rules for monolithic ceramics must include

- simple geometry
- small parts
- uniform wall thickness
- large transition radii
- narrow tolerances only where necessary
- avoid punctual load introduction in order to avoid stress peaks.

Ceramic matrix composites improve the ceramic's tensile strength, enhance its damage tolerance and, thus, makes it more reliable. CMC connects material-typical properties like high temperature or wear resistance with structural possibilities for the manufacturing of thin-walled, large area complex components. However, making of these components for the time being, requires a lot of manpower, for example for draping of the laminate. They are therefore quite costly. During design with CMCs

- use form fit or clamping for load introduction
- at attachment with a substructure: mind the epansion compatibility
- shear loaded components should make use of intralaminar instead of interlaminar load orientation
- when oxidation protection becomes necessary, mind the maximum tolerable component expansion
- chose tolerances so that thermal expansions are compensated
- manufacturing tolerances on the order of metallic sheet processing
- take into account the orthotropy of the material
- for long term high temperature operation, foresee oxidation protection if necessary.

Four examples are given below in which material-tailored thermo-mechanical design was pursued. These are details of the the CETEX tile, the nose cap for the winged demonstrator of the CRV – X-38 –, the nose cap for the European re-entry testbed EXPERT and the faceted thermal protection system of the DLR re-entry vehicles SHEFEX I and SHEFEX II.

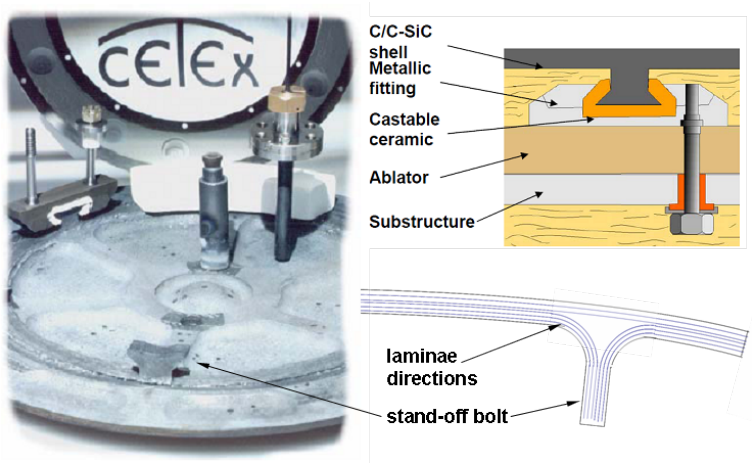

Figure 4.1: Ceramic tile experiment CETEX.

4.1 CETEX

contact: Dr.-Ing. Hermann Hald, German Aerospace Center DLR

CETEX was the first hot structure made of fibre-ceramics in Europe, which was successfully tested during a ballistic re-entry flight. It was a small nose cap for the Japanese-German re-entry capsule EXPRESS, launched in 1995. At a diameter of 300 mm and a typical thickness of 5 mm, CETEX had total mass of approximately 4 kg, 1 kg thereof for the ceramic part itself. For the first time, newly developed ceramic load introductions were used for CETEX. Insulation was accomplished with ZrO_2 felt. CETEX served to a certain extent as carrier platform for the experiments PYREX (IRS, University of Stuttgart) and RAFLEX (HTG, Göttingen) and a temperature measuring technique was developed in co-operation with Kayser-Threde.

During the development of CETEX, qualification tests with material and component samples were accomplished in different plasma wind tunnels. In doing so, temperatures of up to 2700°C were reached in PWK 2 of the Institut für Raumfahrtsysteme (IRS, University of Stuttgart), a number exceeding by far what was regarded at the time the limitation of use of these materials. C/C-SiC behaves like an excellent ablator at these temperatures. Despite technical problems with the Japanese launcher, the capsule performed successful re-entry, although it landed in Ghana instead of in Australia.

Figure 4.1 shows on the left hand side the aft side of ceramic tile. The tile was made from a laminated raw material with a lay-up as shown on the lower right hand side. The stiffening and the stand-offs, as seen in the figure are integral machined. The stand-offs were attached to the vehicle structure by metal fittings from PM2000. Castable fiber ceramic between stand-offs and brackets created form fit and insulated the sub-structure against thermal load. The thermal expansion in this design results in radial displacement of the stand-off in which it is free and expansion can, thus, be compensated. CETEX was exposed to temperatures of approx. 2200°C without problems and the average erosion of approximately 0.9 mm correlates well with the expectations from measured data from plasma wind tunnel tests. Results from the EXPRESS mission formed the technical and political basis for the next stage of development, i.e. the development of the nose cap system of the experimental vehicle X-38 for the later CRV (Crew Return Vehicle) of NASA for the International Space Station ISS.

4.2 X-38 Nose Cap

contact: Hendrik Weihs, German Aerospace Center DLR

X-38 was designed to be a technology demonstrator of NASA for the life boat CRV (Crew Return Vehicle) for the International Space Station ISS. The Institute for Structures and Design was responsible for the construction and the production of the ceramic nose cap of X-38. In January 2001 the flight unit of the nose cap system of the X-38 was delivered to Johnson Space Center of NASA in Houston and installed to the X-38 in October 2001. At the time, the nose cap was fully qualification tested and accepted by NASA. Unfortunately, the project was stopped by NASA because of financing difficulties on their part in 2002 and the X-38, finished by 80% is now stored in Houston.

During re-entry into the atmosphere, the nose cap of X-38 was to experience the highest thermal load of the entire thermal protection system due to its exposed location in the stagnation point of the vehicle. During the approximately 20 minutes of the re-entry phase, surface temperatures of up to 1750°C were expected with a stagnation pressure of 150 hPa.

The nose cap represented an absolute novelty regarding technological requirements. A fiber-ceramic component for thermal loads up to approx. 1750°C had never been planned before with the claim of re-usability. The nose structure of the Space Shuttle, for example, was made of carbon/carbon (C/C) and the temperatures reach only scarcely 1500°C. The shell structure of the X-38 nose cap has been manufactured with the help of the liquid silicon infiltration process (LSI) of DLR. Figure 4.2 shows the die for the draping of the lay-up. X-38 nose cap is made as an integral component by using a special in-situ joining technology for the ceramic fittings, shown in figures 4.2 b). The flight unit of the nose cap, the shell of which is shown in figure 4.2 c) is provided with a silicon carbide oxidation protection coating.

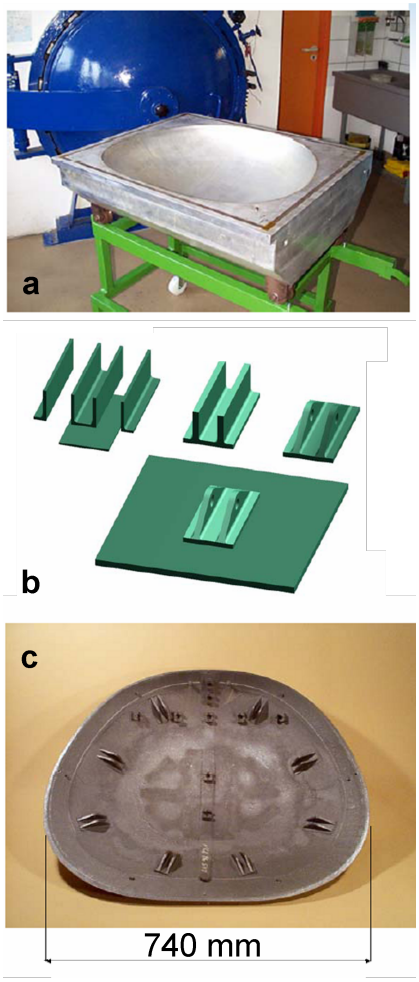

Figure 4.2: X-38 manufacturing: a) laminate die, b) sketch of in-situ joining method, c) photograph of X-38 nose cap.

The connection of the nose shell to the vehicle structure is carried out by eight single fittings. Levers, also made of fiber-ceramic, are connected on the "cold" side to the high temperature-steady (until approx. 1200°C) metal alloy PM 1000. The special arrangement and design of the lever-like attachment system guarantees on the one hand a very good mechanical maximum load and allows on the other hand for unrestricted thermal expansion of the structure, which was predicted to amount to 3 mm with a medium diameter of the shell of 740 mm at the expected temperature level. Had they been rigid attachments, the shell would be destroyed only by the thermal compulsive forces. The pricinple of the lever attachment is sketched in figure 4.3.

The attachment lever itself is shown in figure 4.4. It is attached to the fittings on the nose shell on the hot side and to the metallic fitting on the cold side by bolts also made from C/C-

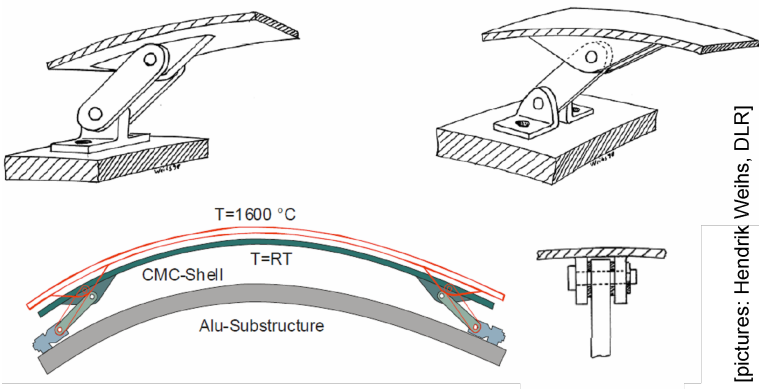

Figure 4.3: Thermal expansion of X-38 nose cap compensated by lever attachment system.

SiC. The bolts are machined out of plates with stacked plies of carbon fiber. This means that the bolt has one direction perpendicular to the laminae and one parallel. In order to make use of intralaminar shear instead of interlaminar shear, the bolt, therefore has to be oriented so that shear is induced intralaminar, as indicated in figure 4.4. In order to hold them in place and not let them vibrate back into bad orientation, the CMC clamp is added that grabs the bolts in groves so they cannot rotate. The clamp, in turn, can only be inserted when the lever is deflected. Therefore, when it is mounted, the clamp cannot slide out but is held in place by the PM 1000-fitting.

Another system integrated in the nose cap system is the pressure measuring system (flush air DATA system, FADS) the data of which is used for attitude control of the vehicle during flight. Pressure is taken from nine crosswide-arranged bores in the nose shell, shown in figure 4.2 c), whereas the pressure transducers are located in the interior of the vehicle. A further component of the nose cap system is a so-called hard seal (rigid seal) connected to the edge of the nose cap and located under the adjoining side panels of the continuative thermal protection system. By interacting with a flexible seal package this seal system prevents the penetration of hot gases under the nose shell at the joints of the individual components.

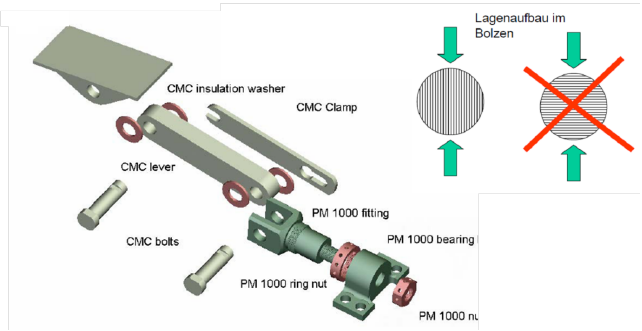

Figure 4.4: Explosion view of X-38 nose cap attachment assembly.

For thermal isolation, a multilevel flexible felt isolation made of oxide fibre-ceramic such as alumina, is laid out between the nose shell and the substructure. The isolation reduces the maximum temperature at the aluminium sub-structure to about 100°C over a thickness of approximately 45 mm. This isolation system was developed and manufactured by Astrium. The entire nose system has a mass of approximately 13.2 kg, in which the nose shell alone accounts for 7 kg. Beside the nose cap itself, the aluminium substructure (MT-Aerospace), the ceramic side panels (ASTRIUM), the so-called chin panel (MT-Aerospace) and ceramic tiles (NASA) were integrated into the qualification unit. For the first time ever, installability and accuracy of fit as well as the functional interaction of all components of the nose section by X-38 could be proven.

4.3 EXPERT Nose Cap

contact: Thomas Reimer, German Aerospace Center

The aim of project EXPERT is to validate aero-thermodynamic models, numeric codes and ground test facilities by representative flight data. This serves for better understanding of the processes in order to improve design of spacecraft. The Institute of Structures and Design of DLR in Stuttgart has built the CMC nose cap for EXPERT. The flight model can be seen in figure 4.5.

EXPERT was concepted to acquire data collected in flight to answer questions on interaction between shock and boundary layer, transition of boundary layer from laminar to turbulent flow, high temperature and gas chemistry effects, and interaction between gas and surface such as catalysis and oxidation. A substantial consequence of this target is the demand of a non-ablative thermal protection system in order to avoid the contamination of the boundary layer by chemical species or solid particles. Therefore, the nose will be made from C/C-SiC as fiber-reinforced ceramic and the fuselage from PM1000, a high temperature nickel based alloy.

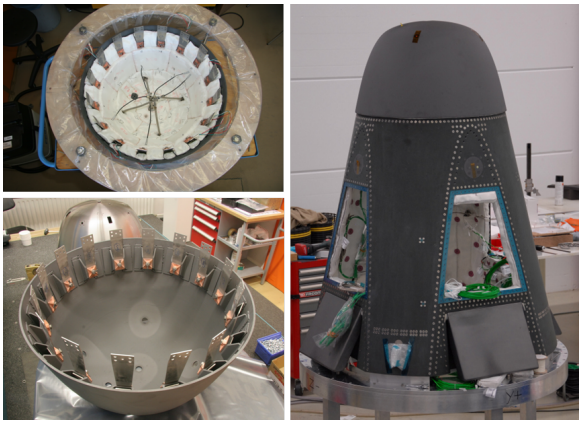

Figure 4.5: Flight model of the EXPERT nose cap. Upper left: instrumented and with insulation pads, lower left: empty with attachment system and substructure (the "colander", behind), right: mounted on EXPERT.

EXPERT is currently planned to be launched in 2012 on a Russian Volna rocket from a submarine in the Pacific and accomplish suborbital flight. The speed of the capsule will amount to a maximum of 5 km/s. The capsule mass adds up to approx. 400 kg. During reentry, the aerodynamic loads will be carried mainly by the ceramic nose. The stagnation pressure is expected as 1.5 bar. The maximum heat flux is foreseen to amount to 1.4 MW/m^2. Thus, temperatures in the range of 2050°C are expected at the stagnation point. The entire re-entry takes approximately 150 seconds.

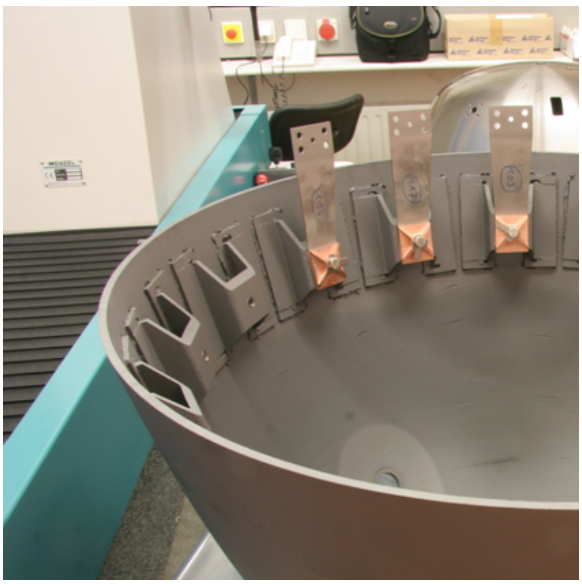

Figure 4.6: Close-up on EXPERT attachment system.

The fiber-ceramic nose houses sensors for the collection of environmental data during reentry by experiments from HTG (Hypersonic Technology Goettingen) and the Institute of Space Systems of the University of Stuttgart. Backface temperature, heat flux and aerodynamic pressure are measured. Furthermore, a window is located in the nose through which a spectrometer collects data on the chemical species present in the boundary layer.

Figure 4.6 shows a close-up on the attachment system. It can be seen left in the picture that so-called “hat profiles” (because they are hat shaped) have been in-situ joined to the edge of the nose cap. On the top (inner side) of the hat, as can be seen further right in the picture, metallic leaf springs from Inconel are attached. At their other end, in turn, they are screwed onto the “colander”, the substructure.

Like in the CETEX and X-38 examples, the challenge for the EXPERT hot structure is its connection to metallic substructural parts. The cold substructure develops almost no thermal expansion while the hot structure, although the CMC material C/C-SiC has typically low expansion, expands by a few millimeters. Thermal expansion on a bell shaped structure as the EXPERT nose cap has two effects for the attachment system. The first one is a radial expansion of the radius, as indicated in the top left in figure 4.7 a). This expansion is compensated for by the flexibility of the Inconel leaf spring. The second effect is the tangential expansion of the material that also drives apart the in-situ joined roots of the hat profile. This is indicated by the two arrows in the lower left of figure 4.7 a).

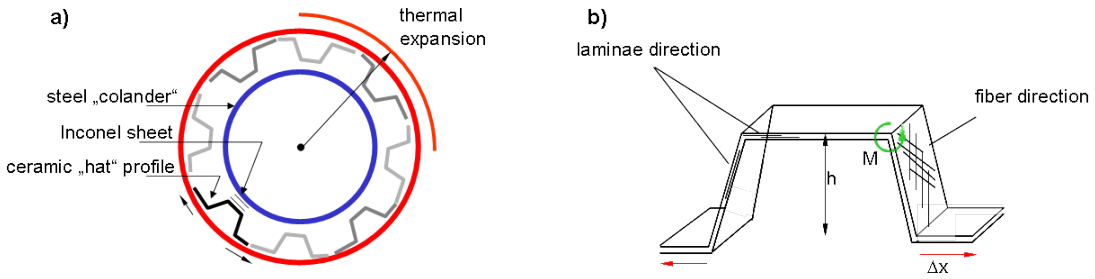

Figure 4.7: a) Sketch of thermal expansion of nose cap (red, hot) and substructure (blue, cold) and b) loads and fiber directions in hat profile.

As already stated, the tangential expansion of the material causes a displacement in the hat profile, as indicated with Δx in figure 4.7 b). The displacement induces a bending moment M in the shoulder of the hat profile, which is linearly dependent on hat height h. The moment, in turn, causes stress σ in the top of the hat, so that the lower laminae are tensile stressed. The green mark indicates the momentum in the shoulder. In order to reduce the stress, the component height could be increased so that the moment would be reduced. However, a compromise had to be found with the integration space and the fact that the profile loses stiffness and torsion or buckling may occur. Another option is to reduce the Young's modulus of the material, since

$$\sigma = E \cdot \epsilon, \tag{4.1}$$

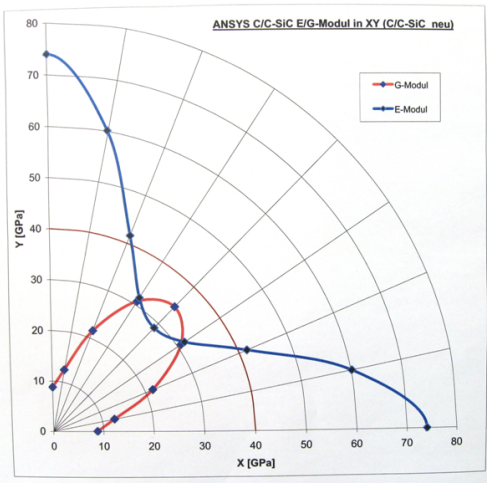

Figure 4.8: Young's modulus for a 0/90°laminate according to load orientation.

by chosing the fiber direction respectively. Figure 4.8 shows Young's modulus for a 0/90°laminate according to load orientation. It can be seen that the modulus is at maximum in fiber directions 0°and 90°and low in ±45°.

By material-tailored design in the EXPERT hat profiles, the modulus was thus reduced, which reduces the moment and finally the stress.

4.4 SHEFEX

SHEFEX I was launched on October 2005. It was a re-entry technology experiment, the foremost purpose of which is to investigate possible new shapes for future cost-effective reentry vehicles. It performed re-entry flight from 90 km down to an altitude of 20 km and telemetred measured temperature, pressure and heat flux data, amongst others. Lessons learned include the comparison of real flight data with numerical simulations and ground testing [21]. A photography is shown in figure 4.9. Considering all experience and collected flight data obtained during the SHEFEX mission in 2005, the test vehicle was re-designed and extended by an active control system, which allows for active aerodynamic control during the re-entry phase [22]. Thus, ceramic based aerodynamic control elements like rudders or flaps, mechanical actuators and an automatic electronic control unit are to be implemented.

The second Sharp Edge Flight Experiment (SHEFEX II) will be launched in spring 2012. SEFEX II uses, again, a shape with faceted surface and a sharp leading edge, thus, reducing the design and manufacturing cost of the thermal protection system [17]. Figure 4.10 shows the geometry of the SHEFEX II fore-body with ogive form and an octagonal cross-section. Other than shape efficiency, the vehicle itself is considered an experimental platform for in-flight relevant re-entry experiments.

The primary substructure of the payload tip consists of an aluminium substructure created by a stiff ribs and stringers set-up. The open volume is then closed by flat aluminium panels which create an inner mould line. These aluminum panels are also used for mounting the TPS facets and experiments. Inside the aluminum substructure, the in-flight measurement infrastructure is integrated. These are thermocouple connection and compensation, pressure transducers, a pyrometer system, data processing boxes, and subsystems for passenger experiments [23].

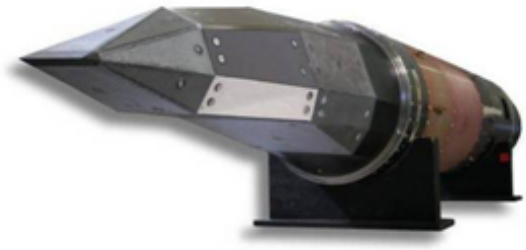

Figure 4.9: SHEFEX I re-entry body with faceted TPS.

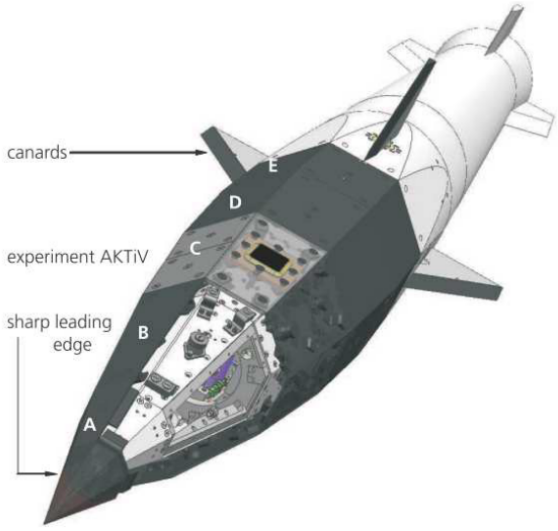

Figure 4.10: SHEFEX II re-entry body.

As explained above, the forebody geometry is symmetrically divided into eight identical facets in circular direction and consists of five segments A through E, as marked in figure 4.10, along the payload tip. Thus, the payload houses 40 single flat areas. Within the flight unit, all facets of the four segments behind the nose are created by single CMC panels.

The basic TPS system facilitates multi-use, low maintenance and rapid turn-around time for the exchange of TPS panels and is shown in figure 4.11. Main element of the concept is the hot C/C-SiC panel, supported in its center with a fixed central post and flexible stand-offs at the four corners, so that the panel's thermal expansion is not suppressed. Between the panel

and the cold aluminum structure, a felt insulation material is laid out. The SHEFEX standard C/C-SiC panel thickness is 3 mm and the insulation thickness is 27 mm. This results in an extremely thin overall TPS thickness of 33 mm including the aluminum panel making room for the payload and instrumentation.

The hot connection of the panels to the CMC stand-off by fasteners in the high temperature regime of up to 1800 K is a key issue of the design concept. These fasteners must facilitate panel attachment and removal having only external access to the TPS. A rivet-type fastening bolt was therefore developed, tested and optimized, combining the function of a screw and a rivet [24, 25]. A total of 180 screw rivets are necessary for the assembly of the flight unit.

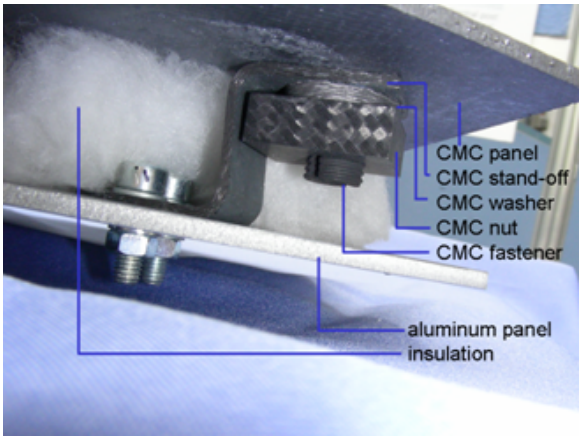

Figure 4.11: SHEFEX II thermal protection system set-up.

The central post and Z-shaped flexible stand-offs are shown in the attachment system of SHEFEX I in figure 4.12. It is also indicated with arrows that the stand-offs in the corners of the panel are flexible in one direction because of their shape. When the hot panel expands, the stand-offs give way in this direction. The center of the panel, however, is fixed with the central post.

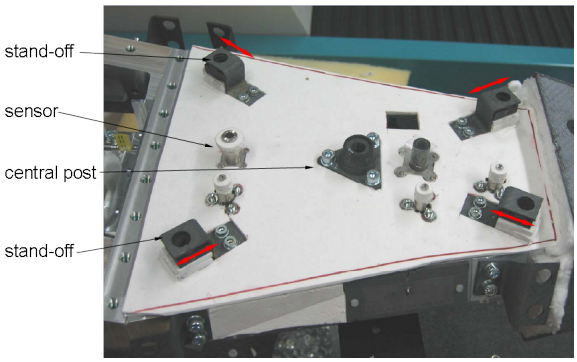

Figure 4.12: SHEFEX attachment system.

SHEFEX II has the same attachment system and it was planned to use the same stand-offs. However, the TPS ceramic panel will reach higher temperatures than those of SHEFEX I because of a faster re-entry. The panel will therfore expand more, causing higher stress in the stand-offs, as indicated in figure 4.13 a). The stand-off is subject to a second load as well, that is the pressure acting on the panels. With the stand-off shaped as in the photograph of figure 4.12 and the sketch in figure 4.13 b), these two loads impose moments and stress in the stand-off in the same direction than the thermal expansion. This means, they add up to an increased load, that was so high in SHEFEX II that it could not be sustained by the stand-off. Its geometry, therefore, had to be adapted.

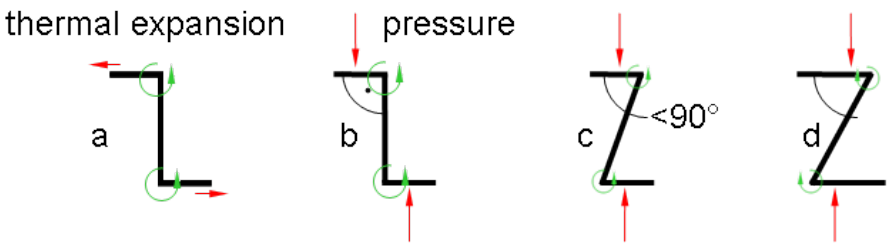

Figure 4.13: a) stand-off for SHEFEX I with load from thermal expansion of panel, b) stand-off for SHEFEX I with load from pressure, c) reduced stress by reduced stand-off angle, d) angle chosen so small that expansion and pressure counteract each other's stress.

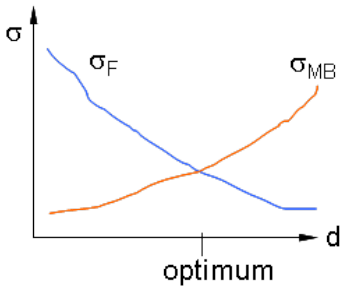

Figure 4.14: Optimized wall thickness.

The analysis is as follows: the moment could be reduced by reducing the levers of the pressure force. The load introduction was therefore brought closer together by reducing the angle of the stand-off below 90°, as shown in figure 4.13 b). With further reducing the angle, it can even be achieved that the moment occurring from the pressure load is oriented in the opposite direction than that one rising from thermal expansion so that the two counteract each other and result in lower stress than with only one of the two loads.

Since the Z-shaped stand-off was already being redesigned for SHEFEX II, the wall thickness was reconsidered, too. The stress σ_{MB} caused by the moments in the shoulders of the stand-off can also be reduced by reducing the stand-off thickness. This is indicated by the orange curve in figure 4.14. However, the flexural stress σ_F in the central leg increases, as indicated by the blue curve. Between two extrema, there is an opposite and it had been found for the stand-offs on SHEFEX with 3 mm.

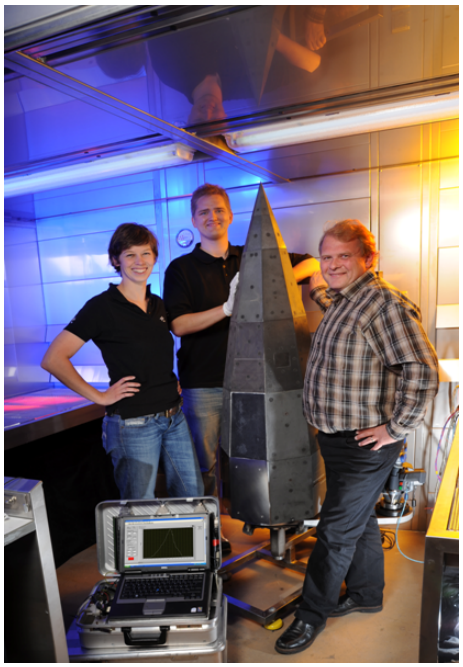

Figure 4.15: SHEFEX II structures team: Hannah Böhrk, Henning Elsäßer and Hendrik Weihs (from left).

5 Sharp Leading Edges

The previous chapters have shown that the outer surface of hypersonic vehicles is subjected to severe aerodynamic heating. It was also shown that especially for sharp edges and at the location of the edge the loads are immense. However, stability of the outer mold line is important since it can impact performance. For example, sharp nose leading edges generate shocks which are necessary to maximize airflow into the engines. Leading edges should therefore not ablate, even when they are expendable parts, but they may have to be actively cooled.

Adding to these issues is the slender aerodynamic shape of minimum drag which provides thin cross-sections at elevated temperatures. One of the primary thermo-mechanical challenges results from large thermal gradients, for example at attachments of hot structures to an airframe, as was described in the former chapter.

Since intakes incorporate leading edges, the present chapter will give an overview over passively and actively cooled leading edges and their design.

5.1 Passively Cooled Leading Edges

5.1.1 SHEFEX Leading Edge

The 1.5-m-long forebody of SHEFEX II has a sharply pointed nose tip made from C/C-SiC. It is shown in fig. 5.1. As discussed above, sharp leading edges are subject to severe aerodynamic heating since the shock remains attached to the pointed structure. The challenge for the designer is thus the choice of cooling method, material choice, attachment, and instrumentation. In case of SHEFEX II, is is sufficient for the nose to be radiation cooled and a loss of up to a few millimeters is tolerated. The nose will be explained here for it's attachment and instrumentation technique. The sharp leading edge of SHEFEX I was attached similarly.

The octahedral pyramid shape is milled from solid material. Problems in terms of delamination are faced when it comes to the manufacturing of high-thickness plates. For this purpose, the sharp leading edge is manufactured by stacking a number of plates in the inter-process state C/C to reach the necessary thickness. Bonded together by in-situ joining, as described above, the leading edge is machined out of the resulting solid block of C/C. It is siliconized in bonded and machined state. The tip radius has been determined after siliconization to approximately 1 mm.

Three thermocouples are mounted in the center of the nose tip to measure the material temperature as close to the fromt as possible, where the aerodynamic shock rises from. Additionally, pressure is measured on each of the eight sides via slender bore holes leading to the aft side of the nose tip. Thermo-couple and pressure bores are electrical discharge machined into the carbon based and therfore electrically conductive material and the pressure bores must be

connected to the pressure transducers by tubes. Eight Inconel tubes are soldered into the ceramic matrix composite in order to make the connection. The soldering junction is manufactured at a processing temperature of ∼900°C. It unsolders at the same temperature. Therefore, care must be taken during the design process that during re-entry the soldering junction remains below this temperature.

The tip is attached to the vehicle by a mount from thin-wall C/C-SiC material, as shown in fig. 5.2. The mount is composed of two half shells, in-situ joined by joining elements, and an inlay, by the joining methos described above. The inlay has four screw-bores through which by means of four C/C-SiC fasteners, the nose tip is attached to the mount. The thin-wall mount, in turn, is attached (again by flexible CMC fasteners) to the aluminum substructure by the CMC stand-offs.

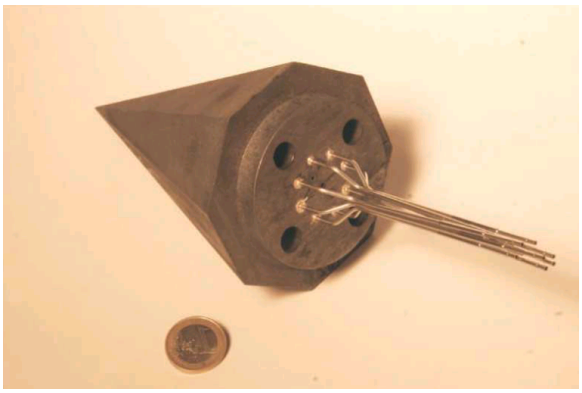

Figure 5.1: SHEFEX II C/C-SiC sharp leading edge with pressure tubing.

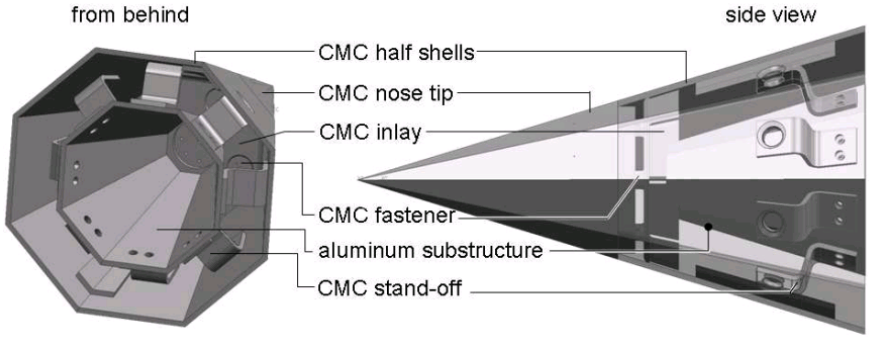

Figure 5.2: SHEFEX II C/C-SiC sharp leading edge design and attachment strategy.

5.1.2 SHEFEX Canard

Another experiment onboard SHEFEX II is dedicated to attitude and roll control during re-entry by means of the so-called canards also shown in fig. 4.10. The canards are mounted onto the flat surfaces of the canard module that transfers the octahedral forebody shape to the cylindric rocket modules. Four independent actuators, mechanically guarded within a secure maximum deflection of 15°, drive the canards. For transportation reasons of the spacecraft to the launch site, they have to be able to be mounted and secured from outside of the canard-module.

Control surfaces are load-bearing and this major difference requires additional consideration during design. Like any structural part in in-flight experiments, the canards have to withstand all thermal and mechanical loads while being lightweight. However, in order to reach sufficient

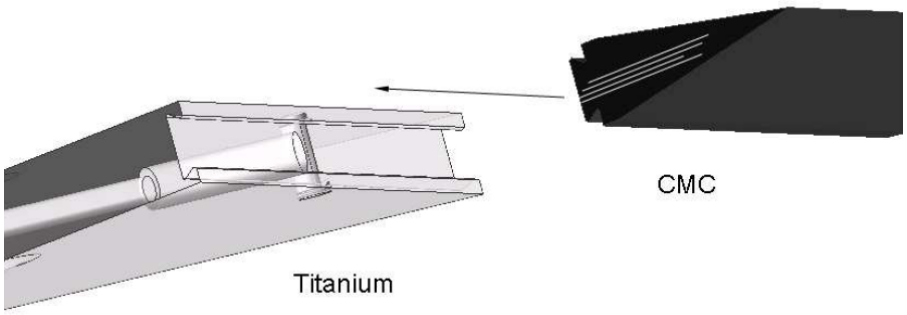

Figure 5.3: Dovetail principle.

efficiency of the canards at altitudes above 60 km with low static air pressure, they are oversized for the lower altitudes. Consequently, high thermo-mechanical loads are encountered at low altitudes of 20 km altitude, which was defined as the end of the experiment. The major challenge of the canard design is thus to withstand the resulting high mechanical load at the canard pivot in combination with the high thermal loads at the leading edges. A hybrid canard design was chosen using a metallic main structure at the pivot and a CMC as leading edge.

The sharp leading edge of the hybrid canard is made from C/C-SiC and the main structure including the pivot is made from titanium. This choice of material combination accounts for similar coefficients of thermal expansion. Titanium moreover has high strength and low density. Figures 3.4 and 3.7 give strength and thermal expansion coefficient for both materials to underline the functionality symbiosis of the hybrid structure. For joining of the two structural parts from CMC and titanium, a dovetail principle is applied as shown in fig. 5.3. It compensates for the remaining difference in thermal expansion by admitting displacement of the components in length direction. In thickness, i.e. out of plane of the C/C-SiC ($\perp$), the thermal expansion coefficients of both materials are comparable, shown in fig. 3.7, guaranteeing a tight conjunction throughout the whole flight. The leading edge's laminae lay-up is also indicated in fig. 5.3. To secure the CMC at the titanium, it is locked with a CMC pin.

As mentioned above, for tranportation reasons, the hybrid structure must allow for mounting with external access only. The titanium part can be slipped onto the canard-module at first followed by sliding in the CMC part and securing it with a pin. The mounting procedure is depicted in fig. 5.4.

The canard lay-out was also carried out for the maximum heat load i.e. at 20 km altitude. The maximum mechanical canard load is 10 kN for a canard angle of 20°[26]. In hypersonic flight, this is equivalent to a pressure difference of 1.8 bar on the canard surface. For proving stability, a finite element analysis was carried out for two cases. The first one is a worst case scenario as in case of a malfunction in the canard actuators in which the canard would keep a constant maximum canard deflection of 15° throughout the entire experiment region. The second one are functional canards with nominal mechanical loads and relatively even thermal load onto both sides of the canard.

For the analysis first a transient thermal analysis for the experiment time can be accomplished, for example with commercial FEM-software. The resulting temperature distribution at an altitude of 20 km and Mach 8 can then be taken to accomplish athermo-mechanical analysis in a second step. Results show that the canard leading edge will most likely be subject to extreme heat load and temperatures [26]. The sharp leading edge is not coated, either, so that active oxidation is expected to a certain amount. This is, however, tolerated, since erosion

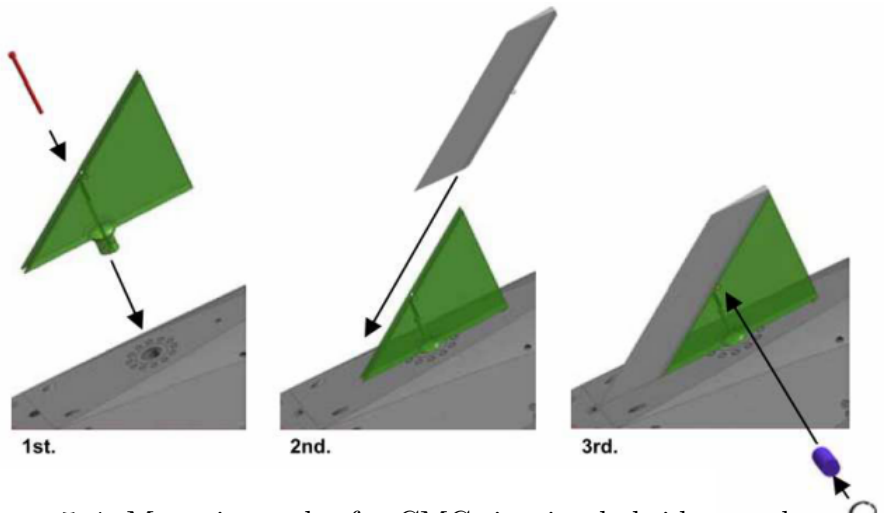

Figure 5.4: Mounting order for CMC-titaniumhybrid canard structure.

is expected to take only a few millimeters of the leading edge. The main titanium structure is also expected to locally overheat, but creep is expected to take place to only a limited extent [26]. Both structural parts are mechanically loaded under their limits by factors of $\gg$1.5. In the titanium structure, the maximum stress appears at the pivot and in the C/C-SiC at the dovetail inner radius. Because of higher coefficients of thermal expansion, the titanium is expected to elongate beyond the C/C-SiC edges and pull the C/C-SiC by frictional effects. The maximum but uncritical load of 45 MPa resulting from this effect is located at the safety pin from figure 5.4.

5.1.3 High Temperature Coatings

Silicon carbide-based coatings enhance oxidation resistivity of a structure. They have a high emission coefficient and can be used up to 1700°C. This is good for blunt re-entry missions, that impose only short exposure time, such as the EXPERT nose cap. On air-breathing vehicles, temperatures however exceed the 1700°C due to high dynamic pressure, velocity and exposure time. Coatings can also be UHTC-coatings or oxydic, as in zirconia. Oxidic coatings are used for resistance to high temperature oxidation and corrosion. Figure 5.5 shows an iridium coated lading edge from [1]. Iriudium is promising as a prtotective layer, because it melts at 2440°C, has verly low oxygen permeability and is unreactive with carbon. When a coating is used, thermal expansion of the coating and the substrate have to be matched. The coating mustn't buckle and spall, it cannot fall off, resulting in oxidation of the substrate.

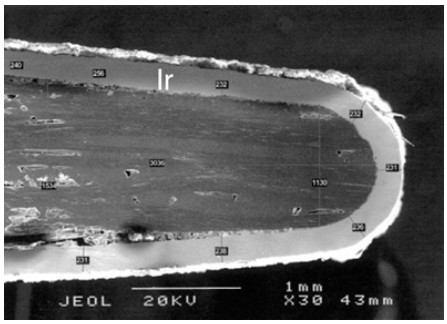

Figure 5.5: Photomicrograph of a cross-section of a C/C leading edge with an iridium (Ir) coating [1].

5.1.4 X-43 Leading Edge

The X-43 was a row of scramjet propulsion test vehicles for an unmanned experimental hypersonic aircraft. It was a single-use vehicle that would crash into the ocean without recovery. Three missions have been carried out. After one failure in which the vehicle had to be destroyed, two other missions have successfully flown in March and November 2004 and made it the fastest free flying air-breathing aircraft in the world. The scramjet operated for approximately 10 seconds, followed by a 10 minute glide and intentional crash.

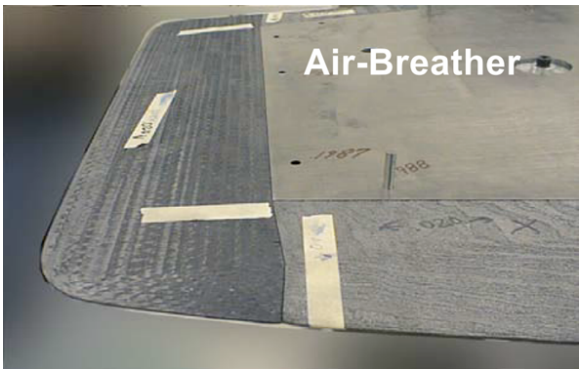

Figure 5.6: The sharp leading edges on the X-43 [1].

Another example of a passive leading-edge design approach is, thus, the X-43 Mach 10 vehicle nose leading edge, which was designed to reach nearly 2200°C during the short 130-second flight. High conductivity fibers have been woven into an unbalanced architecture to help conduct heat away from a leading edge, thus reducing the maximum temperatures. The flight conditions (Mach 10 at 32 km) were simulated in the H2 arc-jet facility at Arnold Engineering and Development Center, Tullahoma, TN. The nose radius for the arc-jet test was 0.76 mm. The heat flux for the test was 14.8 MW/m^2, for 130 s like the original flight time [1].

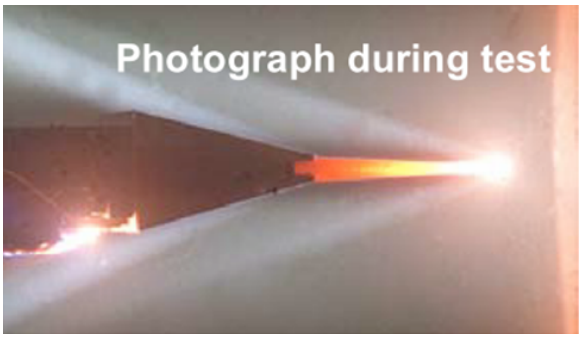

Figure 5.7: Arc-jet coating evaluation of X-43 leading edges [1].

Glass [1] shows a coated leading-edge test article during arc-jet testing in figure 5.7. Figure 5.8 shows a successfully tested specimen and one that failed, where the coating came off and there was severe oxidization of the carbon/carbon substrate. High thermal gradients can result in high thermal stresses, as was the situation on the leading edges of this test article. Thermo-structural modeling predicted the leading edges would fail due to the high compressive thermal stresses resulting from the constraint of the thermal expansion [1]. The primary environment durability challenge is oxidation resistance, which has a major impact on mission life. The number of cycles required under combined loads, inspection and repair, and the ability to predict mission life all present challenges. Figure 5.9 shows a failed test article after severe oxidation during an arc-jet test.

Figure 5.8: Successful test article [1].

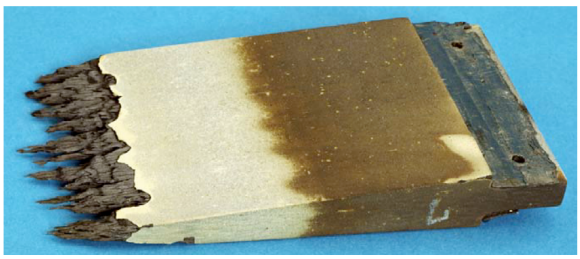

Figure 5.9: Failed test article after severe oxidation during an arc-jet test [1].

5.2 Actively Cooled Leading Edges

When heat fluxes result in temperatures above the multi-use temperature of structures, other approaches need to be evaluated. Below, actively cooled concepts for leading edges are shown. The heat pipe concept and the metallic actively cooled leading edge have been published by D. Glass [1].

The development of leading edges is ongoing and the examples shown here make no claim to be complete. New and improving solutions are, therefore, rather possible.

5.2.1 Heat Pipe-Cooled Leading Edge [1]

Heat-pipe-cooled leading edges, which are semi-passive, utilize heat pipes to reduce leading- edge temperatures below the re-use limits of the materials. A heat pipe is a self-contained, two-phase heat transfer device which is composed of a container, a wick, and a working fluid. Heat input locally to one section of the heat pipe, the evaporator region, is conducted through the container and into the wick/working-fluid matrix, where it is absorbed by the evaporation of the working fluid. The heated vapor flows to a slightly cooler section of the heat pipe where the working fluid condenses and gives up its stored heat. The heat is then conducted through the wick/working-fluid matrix and container and is rejected. The location of the heat pipe where heat is rejected is called the condenser region. The cycle is completed with the return flow of liquid condensate back to the heated region (evaporator) by the capillary pumping action of the wick. During normal operation, heat pipes operate as devices of very high effective thermal conductance and maintain a nearly uniform temperature over the entire heat-pipe length.

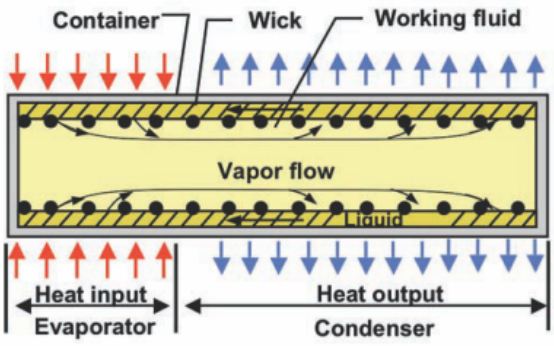

Figure 5.10: Schematic diagram illustrating the operation of a heat pipe [1].

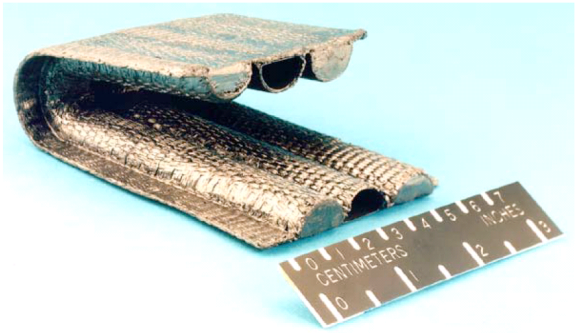

Figure 5.11: Photograph of Mo-Re tube embedded in C/C illustrating the design of a NASP heat-pipe-cooled wing leading edge [1].

Heat pipes provide cooling of stagnation regions by transferring heat nearly isothermally to locations aft of the stagnation region, thus raising the temperature aft of the stagnation region above the local radiation equilibrium temperature. When applied to leading-edge cooling, heat pipes operate by accepting heat at a high rate over a small area near the stagnation region and radiating it at a lower rate over a larger surface area, as shown in Figure 5.10. The arrows in Figure 5.10 indicate the net heat flux. The use of heat pipes results in a nearly isothermal leading-edge surface, thus reducing the temperatures in the stagnation region and raising the temperatures of both the upper and lower aft surfaces.

Heat-pipe-cooled wing leading edges were studied during the National Aerospace Plane (NASP) program. The leading edges had a carbon/carbon structure with Mo-Re heat pipes as the container, shown in Figure 5.11. Three straight Mo-Re heat pipes, approximately 760 mm long, were fabricated and embedded in carbon/carbon. The heat pipes had a D-shaped cross-section and utilized lithium as the working fluid.

Material compatibility and thermal stresses are two of the major challenges with heat pipes embedded in composite materials such as carbon/carbon. Two different materials (carbon and Mo-Re for the container) at elevated temperatures for long durations are problematic. If the Mo-Re is in contact with the carbon/carbon, molycarbides will start to form. The formation of the molycarbides is a function of both time and temperature. Carbon may also diffuse through the Mo-Re into the heat pipe and degrade the heat pipe's operation. This diffusion is also a strong function of both time and temperature. Thermal stresses present another problem. The Mo-Re has a larger coefficient of thermal expansion than C/C, and will thus be constrained by the C/C. Due to the constraint in growth, there is the possibility that the flat section of the heat pipe could buckle during operation. The difficulty here is that good thermal contact (through- the-thickness) is required to transfer the heat from the outer surface into the heat pipe, but a loose fit is desired to minimize thermal stresses due to the mismatch in coefficient of thermal expansion.

5.2.2 Metallic Active-Cooling Leading Edge [1]

For the highest heat fluxes, active cooling is required. Metallic actively-cooled leading edges have been fabricated, and the challenges include hydrogen interaction and multi-cycle life. A photograph of the internal portion of an actively cooled leading edge is shown in Figure 5.12.

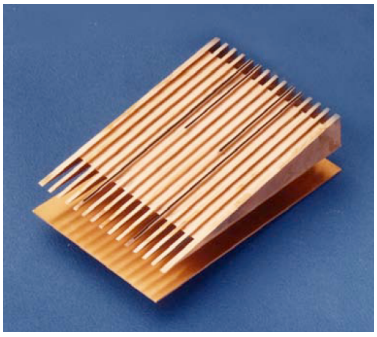

Figure 5.12: Photograph of the internal portion of an actively cooled leading edge as published by Glass.

5.2.3 Transpiration-Cooled Leading Edge

Like the transpiration-cooled acreage TPS experiment AKTiV described in chapter 2, this strategy can also be applied for leading edges. Figure 5.13 shows a sketch in which surround flow and transpiration flow are indicated.

A transpiration-cooled leading edge is foreseen for SHEFEX III. The predecessor, AKTiV, a transpiration cooling experiment on one of the panels of SHEFEX II is ready for flight. The project SHEFEX III will start in 2012 and launch is plannes for 2016. Challenges include the prediction of necessary coolant mass flow distribution over the profile including cooling efficieny in turbulent flow, realization of a graded mass flow rate, attachment of the structure to the vehicle, tightening of the reservoir towards the porous structure, and many other aspects.

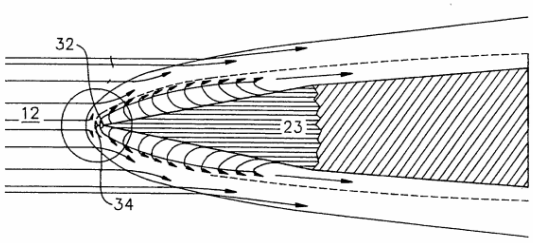

Figure 5.13: Transpiration-cooled Leading Edge as sketched by Bulman.

Literaturverzeichnis

[1] Glass, D.E.: Ceramix Matrix Composite (CMC) Thermal Protection Systems (TPS) and Hot Structures for Hypersonic Vehicles. In: *15th AIAA/DLR/DGLR International Space Planes and Hypersonic Systems and Technologies Conference*. Dayton, USA, May 2008. – AIAA-2008-2682

[2] Oertel Jr., H.: *Aerothermodynamik*. Springer-Verlag, Berlin Heidelberg, 1994

[3] Hirschel, E.H., Zarchan, P.: *Basics of Aerothermodynamics*. Springer, 2006 (Progress in Astronautics and Aeronautics 206)

[4] Longo, J.M.A., Eggers, Th., Gülhan, A., Turner, J., Weihs, H.,: Designing Flight Experiments for Hypersonic Flow Physics. In: *Lecture Series "Flight Experiments for Hypersonic Vehicle Development"*. Brussels, Belgium : RTO AVT VKI Lecture Series, 2005

[5] Strohmeyer, D., Eggers, Th., Haupt, M.: Waverider Aerodynamics and Preliminary Design for Two-Stage-to-Orbit Missions, Part 1. In: *Journal of Spacecraft and Rockets*. 35 (1998), Nr. 4, S. 450–458

[6] Eggers, Th., Novelli, Ph., Haupt, M.: Design Studies of the JAPHAR Experimental Vehicle for Dual Mode Ramjet Demonstration. In: *10th AIAA/NAL/NASDA/ISAS International Space Planes and Hypersonic Systems and Technologies Conference*. Kyoto, Japan, Apr. 2001. – AIAA 2001-1921

[7] Reuther, J., Kinney, D., Smith, S., Kontinos, D. Gage, P., Saunders, D.: A reusable space vehicle design study exploring sharp leading edges. In: *35th AIAA Thermophysics Conference*. Anaheim, CA, Jun. 2001. – AIAA 2001-2884

[8] Arnold, J., Johnson, S., Wercinski, P.: SHARP: NASA's Research and Development Activities in Ultra-High Temperature Ceramic Nose Caps and Leading Edges for Future Space Transportation Vehicles. In: *52nd International Astronautical Congress*. Toulouse, France, Oct. 2001. – IAF paper 01-V.5.02

[9] Böhrk, H., Piol, O., Kuhn, M.: Heat Balance of a Transpiration-Cooled Heat Shield. In: *Journal of Thermophysics and Heat Transfer*. 24 (2010), Nr. 3, S. 581–588

[10] van Driest, E.R.: Investigation of Laminar Boundary Layer in Compressible Fluids using the Crocco Method. In: *Tech. Rep. NACA TN-2597, NACA*. (1952)

[11] van Driest, E.R.: The Problem of Aerodynamic Heating. In: *Aeronautical Engineering Review*. 15 (1956), Nr. 10, S. 26–41

[12] Glass, D.E., Dilley, A.D., Kelly, H.N.: Numerical Analysis of Convection and Transpiration Cooling. In: *Journal of Spacecraft and Rockets*. 38 (2001), S. 15–20

[13] Hald, H.: CMC Materials: from Plasma Channel Testing to Real Capsule Re-Entry. In:

High Temperature Chemical Processes. 3 (1994), April, S. 153–165

[14] Hald, H.: *Faserkeramiken für heiße Strukturen von Wiedereintrittsfahrzeugen Simulation, Test und Vergleich mit experimentellen Flugdaten*, Universität Stuttgart, Fak. Luft- und Raumfahrttechnik, Dissertation, 2001

[15] Reimer, T.: The KERAMIK Thermal Protection System Experiment on the FOTON-M2 Mission. In: *5th European Workshop on Thermal Protection Systems & Hot Structures Conference Proceedings*. Noordwijk, The Netherlands, May 2006. – SP-631

[16] Eggers, T., Longo, J., Turner, J., Jung, W., Hörschgen, M., Stamminger, A., Gülhan, A., Siebe, F., Requardt, G., Laux, T., Reimer, T., Weihs, H.: The SHEFEX Flight Experiment – Pathfinder Experiment A for a Sky Based Test Facility. In: *14th AIAA Spaceplane Systems and Technologies Conference*. Canberra, Australia, Nov. 2006

[17] Gülhan, A., Siebe, F., Weihs, H., Laux, T., Longo, J., Eggers, T., Turner, J., Hörschgen, M.: The Sharp Edge Flight Experiment – a mission overview. In: *5th European Workshop on Thermal Protection Systems & Hot Structures Conference Proceedings*. Noordwijk, The Netherlands, May 2006. – SP-631

[18] Weihs, H., Hald, H., Reimer, T., Fischer, I.: Development of a CMC Nose Cap for X-38. In: *52nd International Astronautical Congress*. Toulouse, France, Oct. 2001

[19] Reimer, T., Laux, T.: Thermal and Mechanical Design of the Expert C/C-SiC Nose. In: *5th European Workshop on Thermal Protection Systems & Hot Structures Conference Proceedings*. Noordwijk, The Netherlands, May 2006. – SP-631

[20] Krenkel W.: *Keramische Verbundwerkstoffe*. Wiley-VCH, Weinheim, 2002. – [in German]

[21] Barth, T.: Considerations on CFD Modeling for the Design of Re-Entry VehiclesAero- and Thermodynamic Analysis of SHEFEX I. In: *Engineering Applications of Computational Fluid Mechanics*. 2 (2008), S. 76–84

[22] Weihs, H., Longo, J., Turner, J.: The Sharp Edge Flight Experminet SHEFEX II, a Mission Overview and Status. In: *15th AIAA International Space Planes and Hypersonic Systems and Technologies Conference*. Dayton, Ohio, Apr. 2008. – AIAA-2008-2542

[23] Weihs, H., Turner, J., Longo, J.M.: The Sharp Edge Flight Experiment SHEFEX II, a Mission Overview and Status. In: *15th AIAA/DLR/DGLR International Space Planes and Hypersonic Systems and Technologies Conference*. Dayton, USA, May 2008

[24] Ortelt, M., Rühle, F., Hald, H., Weihs, H.: Dynamic qualification of a new CMC fastener. In: *4th international conference on high temperature ceramic matrix composites*. Munich, Germany, 2001

[25] Böhrk, H., Beyermann, U.: Secure tightening of a CMC fastener for the heat shield of re-entry vehicles. In: *Composite Structures*. 92 (2010), Jan., Nr. 1, S. 107–112

[26] Elsässer,H., Weihs, H.: Design and Thermo-Mechanical Analysis of the Aerodynamic Control Surfaces on SHEFEX-II. In: *6th European Workshop on Thermal Protection Systems & Hot Structures Conference Proceedings*. Stuttgart, Germany, Apr. 2009